Title

Neutron irradiation hardening and microstructure changes in Fe-Mn binary alloys

Authors

Kiyohiro Yabuuchi[a*], Masashi Saito[a], Ryuta Kasada[b], Akihiko Kimura[a]

Affiliation

[a] Graduate School of Energy Science, Kyoto University, Uji, Kyoto, Japan

[b] Institute of Advanced Energy, Kyoto University, Uji, Kyoto, Japan

Corresponding Author

Name: Kiyohiro Yabuuchi

Postal address: Gokasho, Uji, Kyoto 611-0011, Japan

Telephone number: +81-774-38-3478

Fax number: +81-774-38-3479

E-mail address: k-yabuuchi@iae.kyoto-u.ac.jp

Abstract

Irradiation hardening and microstructure changes in Fe-Mn binary alloys were investigated after neutron irradiation at 290 ºC and up to 0.13 dpa. Significant irradiation hardening comparable to that of Fe-1 at.%Cu alloy was observed in Fe-1 at.%Mn alloy. Manganese increases the number density of dislocation loops, which contributed to the observed irradiation hardening. Manganese serves as a nucleus of the loop by trapping interstitial atoms and clusters, preventing 1D motion of the loops.

Keywords

irradiation hardening, microstructural evolution, binary alloy, Mn effect, matrix defects

1. Introduction

Neutron irradiation hardening of reactor pressure vessel steels (RPVS) is considered to occur as a result of irradiation-induced microstructures such as dislocation loops, solute clusters, and microvoids. Since solute atoms may interact with point defects induced by neutron irradiation, microstructure evolution under irradiation would be affected by the alloying elements of steels. Manganese is a major solute in typical RPVS that is considered to play key roles in microstructure evolution under neutron irradiation. However, the role of Mn in irradiation hardening of simple iron binary alloys and RPVS has not yet been elucidated.

The interactions between solute atoms and point defects have been studied for iron-based model alloys using low-temperature electron irradiation experiments [1-3], and the results of these studies have suggested that undersized solute atoms combine with self-interstitials and the resulting mixed dumbbells are more thermally stable than self-interstitials. However, the interaction between solute atoms, especially 3d transition elements, and point defects in bcc Fe could not be explained in terms of size factor. The magnetic properties of solute atoms have also been assumed to be important, and recent ab-initio calculations support this assumption [4-6]. Nevertheless, there is still a great deal of uncertainty regarding whether there is a significant difference in the interactions of Mn with vacancy and interstitial-type defects, even though Mn atoms are slightly oversized [6].

The interaction of solute atoms with point defects leads to two types of microstructure evolutions, i.e., the formation of solute-rich precipitates and enhancement/inhibition of the formation of point defect clusters. It is well known that

significant irradiation hardening occurs in high-Cu RPVS caused by Cu rich precipitates (CRPs), which primarily consist of oversaturated Cu [7-10]. Recently, Mn-Ni-rich precipitates (MNPs) were also observed in low-Cu RPVS [11-13]. Three-dimensional atom-prove tomography (3DAP) and small angle neutron scattering (SANS) have revealed the nature of solute-rich clusters. Solute atoms also influence the formation of point defect clusters, which are well known as interstitial loops and voids. Although it is difficult to reveal the nature of point defect clusters less than 1 nm by transmission electron microscopy (TEM), vacancy clusters can be pursued by positron annihilation spectroscopy (PAS). However, only a few studies have reported the irradiation hardening and microstructure changes in Fe-Mn alloys [14, 15]. Furthermore, the irradiation dose that the materials used in previous studies were subjected to was so low that the effect of Mn probably could not form a sufficient number of point defect clusters.

In the present study, neutron irradiation hardening and microstructure changes in Fe-Mn binary alloy were investigated to clarify the effects of Mn on the irradiation hardening of bcc Fe.

2. Experimental Methods

2.1. Materials and irradiation conditions

The materials used were Fe-0.1Mn, Fe-1Mn, and Fe-1.4Mn (at.%) alloys, as well as pure Fe and Fe-1Cu (at.%) for comparison. The chemical compositions of the materials used are listed in Table 1. Alloy button ingots were produced by the arc-melting method in Ar gas atmosphere using a copper hearth. The alloy buttons were first homogenized at 1000 ºC for 24 h and then at 825 ºC for 48 h, after which they were

furnace cooled. The buttons were then cold rolled into 0.3-mm-thick sheets without annealing. Tensile specimens with a gage geometry of 1.2-mm wide × 5.0-mm long × 0.25-mm thick and disk-shaped specimens with a diameter of 3 mm for transmission electron microscopy (TEM) were punched out. All specimens were finally recrystallized at 825 ºC for 0.5 h, after which they were quenched in ice water.

Neutron irradiations were conducted in the Japan Materials Testing Reactor (JMTR) under the conditions listed in Table 2. The irradiation temperatures were monitored and controlled at 290 ± 1 ºC.

2.2. Post-irradiation experiments

Tensile tests were conducted at room temperature (RT) at a crosshead speed of 0.2 mm/min. Irradiation hardening was measured as the difference in the yield stress before and after irradiation; $\Delta\sigma_y = \sigma_{y,irr} - \sigma_{y,unirr}$. The yield stress was defined as the 0.2% offset value from the straight line of elastic deformation in the stress strain curve. The yield stress was the average of the three tensile tests.

The microstructure of the materials was observed by TEM (JEM-2010) at an acceleration voltage of 200 kV. Thin foils were prepared using a focused ion beam (FIB) system and an ultralow-energy Ar ion beam sputtering system (Technorg-Linda GentleMill). Radiation-induced defects were observed by a weak beam technique. The Burgers vector $\boldsymbol{b}$ of dislocation loops was determined by $\boldsymbol{g}\cdot\boldsymbol{b}$ analysis. It was assumed that only ½<111> loops and <100> loops existed in the irradiated specimens. The nature of the loops was determined by the inside-outside technique [16]. The foil thickness was measured by the convergent beam electron diffraction (CBED) method.

3. Results

3.1. Irradiation hardening and microstructure changes in Fe-Mn alloys

The effect of neutron irradiation (0.13 dpa) on the tensile stress-strain behavior of Fe-1Mn alloy is shown in Fig. 1, as well as that on the stress-strain behavior of pure Fe and Fe-1Cu alloy for comparison. Fe-1Mn alloy showed much larger irradiation hardening ($\Delta\sigma_y$ = 344 MPa) than pure-Fe ($\Delta\sigma_y$ = 83 MPa). The large hardening in Fe-1Mn alloy was comparable to that of Fe-1Cu alloy but was accompanied by a loss of elongation as usual. The irradiation hardening of the Fe-1Cu alloy was considered to be due to CRP [7-10].

Fig. 2 shows the irradiation hardening, $\Delta\sigma_{y,}$ as a function of the square root of dpa for pure-Fe, Fe-1Mn, and Fe-1Cu alloys, as well as the results reported by Alexander et al. [15]. It should be noted that the $\Delta\sigma_y$ of Fe-1Mn alloy abruptly increases over around 0.06 dpa, although there is data scatter. Mn appears to have no effect below 0.06 dpa. The $\Delta\sigma_y$ of the Fe-1Cu alloy exhibited a typical behavior of irradiation hardening in that it increased and then became saturated in response to lower irradiation doses [7, 9]. The $\Delta\sigma_y$ of pure Fe appears to show a linear dependence on $(\text{dpa})^{1/2}$.

The dependence of irradiation hardening ($\Delta\sigma_y$) on the Mn contents is shown in Fig. 3. Irradiation hardening increased with the increase in the Mn contents. The $\Delta\sigma_y$ of Fe-0.1Mn alloy is almost the same as that of pure-Fe, suggesting that there is a threshold Mn content to enhance irradiation hardening.

Figs. 4 and 5 show the TEM micrographs of the same area observed under different diffraction conditions for pure-Fe and Fe-1.4Mn alloy, respectively, irradiated to 0.09 dpa (04M-17U). Bright and weak-beam dark field images obtained using different $\boldsymbol{g}$ vectors are shown in the micrograph. Table 3 is the $\boldsymbol{g}\cdot\boldsymbol{b}$ table, which was

used to identify the nature of the loops. Examples of $\boldsymbol{g}\cdot\boldsymbol{b}$ analysis are shown as circles A and B in the micrographs. In Fig. 4, the loop indicated by A can be found in all micrographs and is identified as the $\frac{1}{2}[1\bar{1}1]$ loop according to Table 3. Conversely, the loop indicated by B can be found in b) and f), but not in d), as indicated by the dotted circle. Thus, the loop is identified as the $[0\bar{1}0]$ loop.

All dislocation loops were identified by this method. The densities of the ½<111> loop and the <100> loop in pure Fe were found to be 2.4×10^{21} m^{-3} and 2.3×10^{21} m^{-3}, respectively. The total density and the average diameter were found to be 4.7×10^{21} m^{-3} and 11.1 nm, respectively. The inside-outside technique revealed that all the loops are interstitial-type dislocation loops. In the case of the Fe-1.4Mn alloy, the weak-beam dark field images reflect the effects of oxidation of the specimen surface; therefore, quantitative examination was conducted for both the bright and the dark field images. The densities of the ½<111> loop and the <100> loop in the Fe-1.4Mn alloy were found to be 1.1×10^{22} m^{-3} and 1.0×10^{22} m^{-3}, respectively. The total density and the average diameter were 2.1×10^{22} m^{-3} and 9.9 nm, respectively. It could not be determined whether the ½<111> loops were interstitial-type or vacancy–type loops using the diffraction vectors in Table 3; however, the <100> loops was identified as the interstitial-type loops.

Based on the numerical data obtained above, irradiation hardening could be estimated by the Orowan-type mechanism, which is expressed as follows:

$$\Delta\sigma_{y(calc.)} = \alpha M \mu b (N \cdot d)^{0.5} \text{ ---------- (1)}$$

where α is the strength factor, which is 0.25–0.6 for dislocation loops [17-19]; M is the

Taylor factor, whose reasonable value for bcc materials is 3.06 [20]; μ is the shear modulus; b is the magnitude of Burgers vector; and N and d are the number density and the average diameter of the loops, respectively. In the present study, α was set to 0.15 for pure-Fe and 0.37 for the Fe-1.4Mn alloy to apply the calculated values to the results of the tensile tests. It can be seen that the loops are able to account for the observed irradiation hardening based on the Orowan-type dislocation barrier mechanism. The difference in the strength factor between pure-Fe and Fe-1.4 Mn alloy can be interpreted in terms of barrier strengthening by the trapping of Mn atoms at the core of the dislocation loops, which increases the interaction force with moving dislocations.

3.2. Mechanism of Mn effects

In a previous study [21], irradiation hardening of neutron-irradiated Fe-1at.%Cr, Fe-1at.%Ni, and Fe-1at.%Mo alloys was investigated, and no significant irradiation hardening was observed in these alloys, suggesting that Mn atoms play a different role in the formation of radiation-induced defect structures among the other alloying elements. In an ab-initio study conducted by Olsson et al. [6], the binding energies of Mn atoms was rather high, containing both a vacancy and a self-interstitial atom, which is only characteristic of Mn atoms, but not other alloy elements having a high binding energy only with vacancy. It was also shown that the interaction between 3d transition elements and point defects in bcc Fe cannot be accounted for only by the atomic size factor owing to the strong magnetic coupling of the 3d elements. This is especially true for Mn, which showed the greatest deviation from the model, apparently as a result of its electronic structure effects being closely linked to its half-filled d-band. It is expected that this unique property of Mn was a result of the difference in the irradiation

hardening behavior and microstructure changes among Fe-based binary alloys.

According to the tensile test results and the ab-initio study, the characteristic irradiation hardening in Fe-Mn alloys can be attributed to the strong interaction of Mn atoms with interstitial atoms. Manganese atoms behave as the nuclei of the loops by trapping interstitial atoms and interstitial clusters generated by cascades. Moreover, Mn impedes the one-dimensional motion of the interstitial loops. As a result, a high density of loops was observed in irradiated Fe-Mn alloys.

Based on the discussion above, the dose dependence of irradiation hardening of Fe-Mn alloys can be interpreted in terms of breaking out of the trapping capacity of Mn atoms for interstitial atoms. Interstitial atoms and their small clusters are trapped by Mn atoms in solution, which prevents the interstitial-type loops from growing to a size sufficient to cause hardening below 0.06 dpa, even though a high density of defects is stored in the matrix. Above a certain damage level, i.e., around 0.06 dpa in the present case, the number of trapped interstitial atoms per Mn atom increases with dose because there would be no Mn atoms free from interstitial atoms. Thus, the interstitial clusters at Mn atoms grow to a size sufficient to contribute to irradiation hardening, resulting in an abrupt increase in hardening. The dependence of irradiation hardening on Mn content can also be interpreted in terms of the trapping capacity of interstitials atoms by Mn atoms.

4. Conclusions

The roles of Mn in neutron irradiation hardening and microstructure changes in bcc Fe were investigated after irradiation at 290 °C at doses ranging from 4.5×10^{-3} dpa to 0.13 dpa. The main results were as follows:

1) Fe-1at.%Mn alloy shows much larger irradiation hardening ($\Delta\sigma_y$= 344 MPa) than pure-Fe ($\Delta\sigma_y$ = 83 MPa). The large hardening in Fe-1Mn alloy was comparable to that of Fe-1Cu alloy but was accompanied by a loss of elongation as usual.

2) Irradiation hardening increases as the Mn contents increase. It appears that there is a threshold Mn content to cause such a great increase in irradiation hardening.

3) Mn increases the number density of dislocation loops, which contribute to irradiation hardening. In particular, Mn atoms behave as nuclei of the loops by trapping the interstitial atoms and interstitial clusters generated by cascades.

4) The uniqueness of the effects of Mn in the electronic structure is closely linked to its half-filled d-band and may be attributed to the difference in irradiation hardening and microstructure changes among Fe-based binary alloys.

Acknowledgements

This work was supported by a Grant-in-Aid for JSPS Fellows. The authors are grateful to Mr. Narui, Mr. Yamazaki and the staff of the Oarai Branch of the Institute for Materials Research for fruitful discussions on the irradiation condition.

References

[1] F. Maury, A. Lucassoon, P. Lucasson, Y. Loreaux, P. Moser, J. Phys. F: Met. Phys. 16 (1986) 523-541.

[2] E. Kuramoto, Y. Takano, N. Kikuchi, M. Takenaka, J. Nucl. Mater. 141-143 (1986) 829-836.

[3] S. Takaki, J. Fuss, H. Kugler, U. Dedek, H. Schultz, Radiation Effects 79 (1983) 87-122.

[4] C. Domain, C.S. Becquart, Phys. Rev. B 65 (2001) 024103.

[5] D. Nguyen-Manh, A.P. Horsfield, S.L. Dudarev, Phys. Rev. B 73 (2006) 020101.

[6] P. Olsson, T.P.C. Klaver, C. Domain, Phys. Rev. B 81 (2010) 054102.

[7] M. Akamatsu, J.C. Van Duysen, P. Pareige, P. Auger, J. Nucle. Mater. 225 (1995) 192-195.

[8] P. Auger, P. Pareige, S. Welzeland, J-C. Van Duysen, J. Nucl. Mater. 280 (2000) 331.

[9] T. Tobita, M. Suzuki, A. Iwase, K. Aizawa, J. Nucl. Mater. 299 (2001) 267-270.

[10] T. Kudo, R. Kasada, A. Kimura, K. Hono, K. Fukuya, H. Matsui, Mater. Trans. 45 (2004) 338-341.

[11] G.R. Odette, B.D. Wirth, J. Nucl. Mater. 251 (1997) 157-171.

[12] S.C. Glade, B.D. Wirth, G.R. Odette, P. Asoka-Kumar, J. Nucl. Mater. 351 (2006) 197-208.

[13] M.K. Miller, A.A. Chernobaeva, Y.I. Shtrombakh, K.F. Russell, R.K. Nanstad, D.Y. Erak, O.O. Zabusov, J. Nucl. Mater. 385 (2009) 615-622.

[14] T. Takeyama, S. Ohnuki, H. Takahashi, Trans. ISIJ 21 (1981) 326-331.

[15] D.E. Alexander, L.E. Rehn, G.R. Odette, G.E. Lucas, D. Klingensmith, D. Gragg, 9th International Symposium on Environmental Degradation of Materials in Nuclear Power Systems – Water Reactors, (1999) pp. 827-833.

[16] M.L. Jenkins, M.A. Kirk, Characterization of Radiation Damage by Transmission Electron Microscopy, Institute of Physics, 2001.

[17] G.S. Was, Fundamentals of Radiation Materials Science, Springer, 2007, p. 606.

[18] A.C. Nicol, M.L. Jenkins, M.A. Kirk, Mat. Res. Soc. Symp. 650 (2001) R1.3.1.

[19] N. Hashimoto, S.J. Zinkle, R.L. Klueh, A.F. Rowcliffe, K. Shiba, Mat. Res. Soc.

Symp. 650 (2001) R1.10.1.
[20] R.E. Stoller, S.J. Zinkle, J. Nucl. Mater. 283-287 (2000) 349-352.
[21] K. Yabuuchi, M. Saito, R. Kasada, A. Kimura, Mater. Sci. Forum. 654-656 (2010) 2911-2914.

Tables

Table 1 Chemical compositions of pure-Fe, Fe-Mn, and Fe-Cu binary alloys

Material	C	N	O	Mn	Ni	Cu	Fe
				(at.%)			
Pure-Fe	0.0042	0.0015	0.24	<0.00051	<0.00048	<0.00088	balance
Fe-0.1Mn	0.0065	0.0028	0.24	0.095	<0.00048	<0.00088	balance
Fe-1Mn	0.0049	0.0020	0.23	0.95	<0.00048	<0.00088	balance
Fe-1.5Mn	0.0065	0.0024	0.26	1.44	<0.00048	<0.00088	balance
Fe-1Cu	0.00093	0.0024	0.18	-	-	0.94	balance

Table 2 Neutron irradiation conditions (JMTR)

Capsule No.	Fluence (>1MeV, 10^{19} n/cm^2)	Flux (1MeV, 10^{12} n/cm^2/s)	Damage Level (dpa)	Damage Rate (dpa/s)	Irradiation Time (hour)	Irradiation Temperature (°C)
01M-02U	5.6	15	0.084	2.30E-08	1032	290 ± 1
02M-52U	4.5	8.6	0.068	1.30E-08	1461	290 ± 1
02M-54U	8.5	17	0.13	2.60E-08	1384	290 ± 1
03M-65U	0.3	1.2	0.0045	1.90E-09	674	290 ± 1
04M-15U	4.3	8.7	0.065	1.30E-08	1367	290 ± 1
04M-16U	7.5	14	0.11	2.30E-08	1403	290 ± 1
04M-17U	6	6	0.09	9.00E-09	2766	290 ± 1
05M-16U	5.7	11	0.086	1.70E-08	1422	290 ± 1

Table 3 A $\boldsymbol{g}\cdot\boldsymbol{b}$ table for determination of Burgers vector of the dislocation loops

g/b	½[111]	½[11$\bar{1}$]	½[1$\bar{1}$1]	½[$\bar{1}$11]	[100]	[010]	[001]
$\bar{1}$10	0	0	-2	2	-1	1	0
200	2	2	2	-2	2	0	0
110	2	2	0	0	1	1	0
0$\bar{1}$1	0	-2	2	0	0	-1	1

Figure captions

Fig. 1 Tensile stress strain curves of pure-Fe, Fe-1Mn, and Fe-1Cu alloys before and after neutron irradiation at 290 °C to 0.13 dpa (02M-54U).

Fig. 2 $\Delta\sigma_y$ of pure-Fe, Fe-1Mn, and Fe-1Cu as a function of $(dpa)^{1/2}$, as well as the results reported by D.E. Alexander et al. [9].

Fig. 3 $\Delta\sigma_y$ as a function of Mn content for pure-Fe, Fe-0.1Mn, Fe-1Mn, and Fe-1.4Mn irradiated to 0.09 dpa (04M-17U).

Fig. 4 TEM micrographs of the same area of pure-Fe irradiated to 0.09 dpa (04M-17U); bright and dark field images using (a, b) $\boldsymbol{g} = \bar{1}10$ close to the [001] pole, (c, d) $\boldsymbol{g} = 200$ close to the [001] pole, and (e, f) $\boldsymbol{g} = 0\bar{1}1$ close to the [011] pole.

Fig. 5 TEM micrographs of the same area of Fe-1.4Mn irradiated to 0.09 dpa (04M-17U); bright and dark field images using (a, b) $\boldsymbol{g} = \bar{1}10$, (c, d) $\boldsymbol{g} = 200$, and (e, f) $\boldsymbol{g} = 110$ close to the [001] pole.

Fig. 1

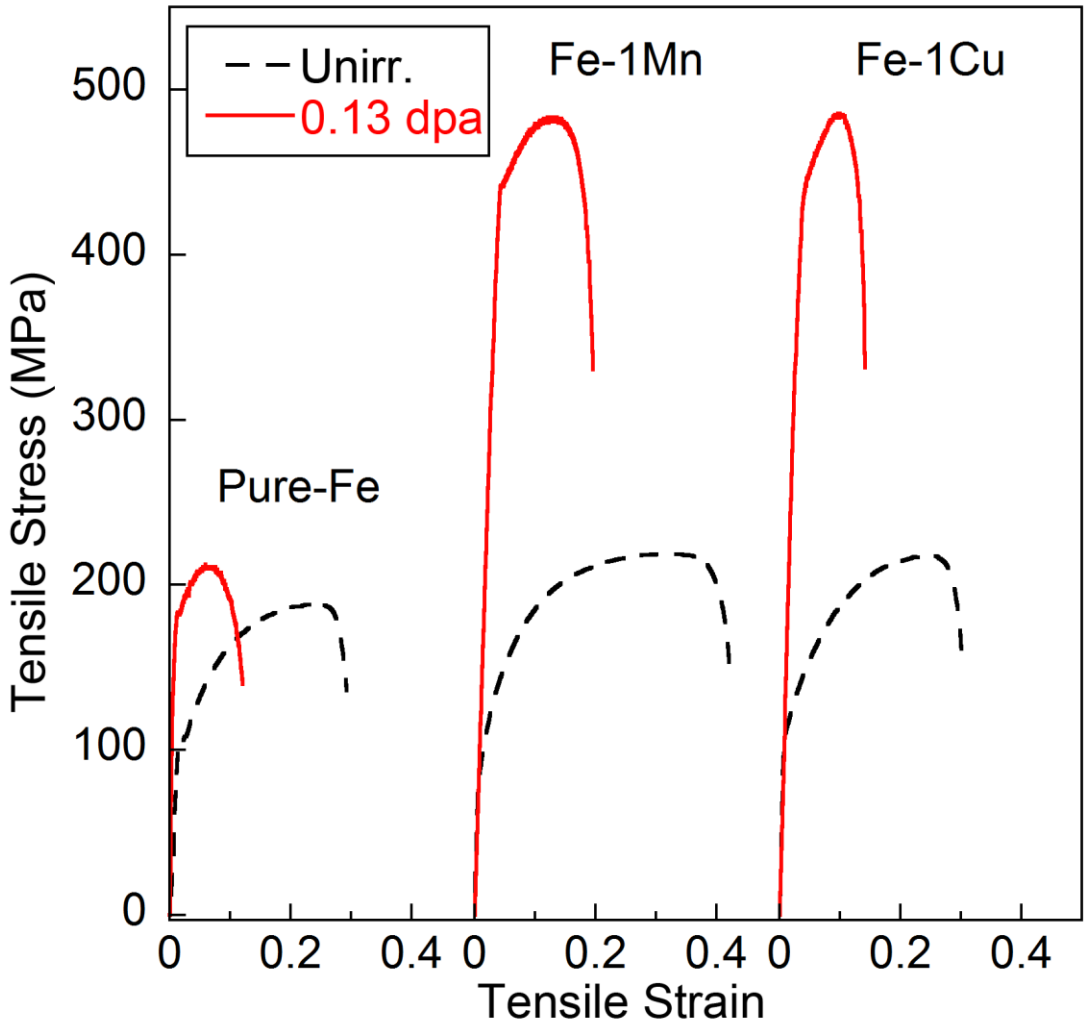
Unirr.
0.13 dpa
Pure-Fe
Fe-1Mn
Fe-1Cu
Tensile Stress (MPa)
Tensile Strain
0
100
200
300
400
500
0
0.2
0.4

Fig. 2

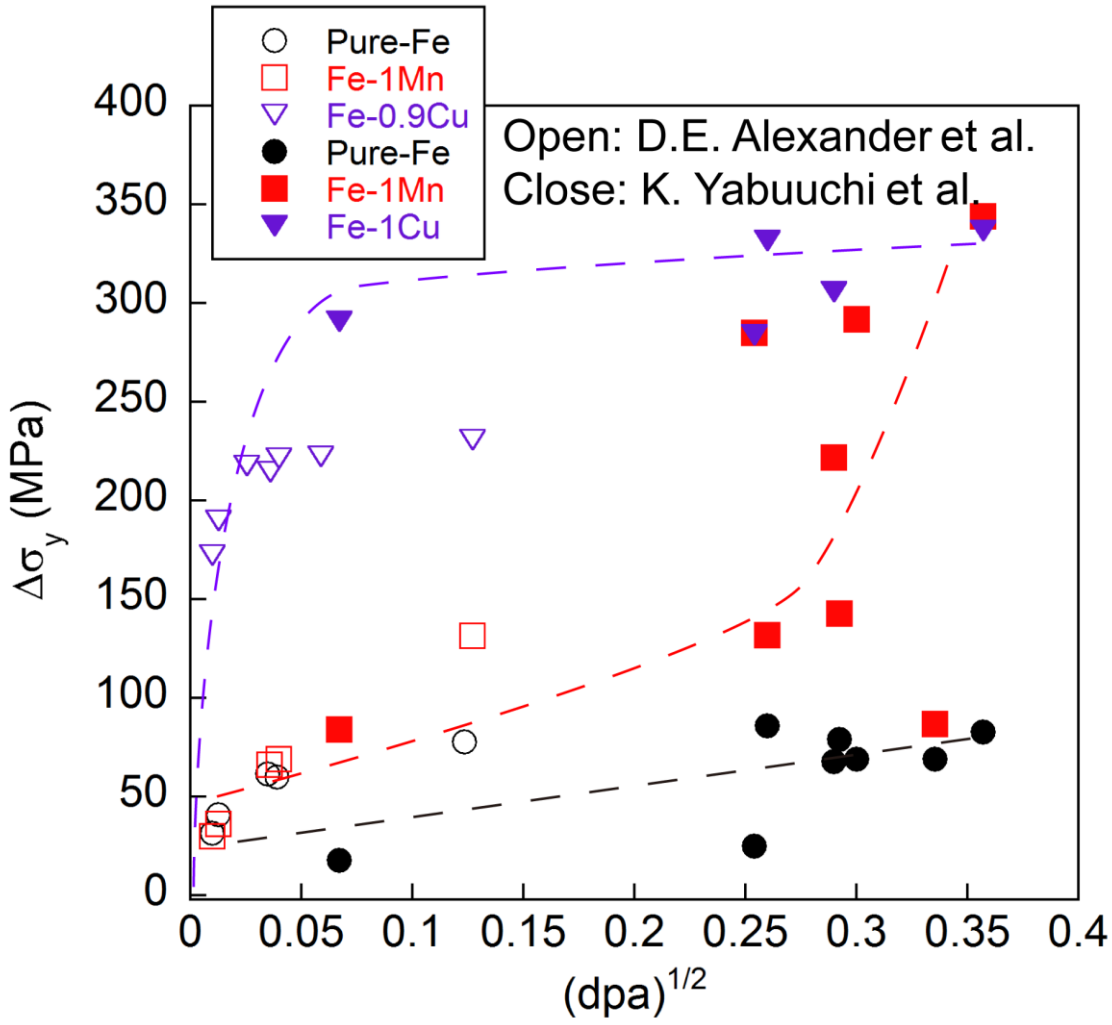
Pure-Fe
Fe-1Mn
Fe-0.9Cu
Pure-Fe
Fe-1Mn
Fe-1Cu
Open: D.E. Alexander et al.
Close: K. Yabuuchi et al.
Δσy (MPa)
(dpa)1/2
0
50
100
150
200
250
300
350
400
0
0.05
0.1
0.15
0.2
0.25
0.3
0.35
0.4

Fig. 3

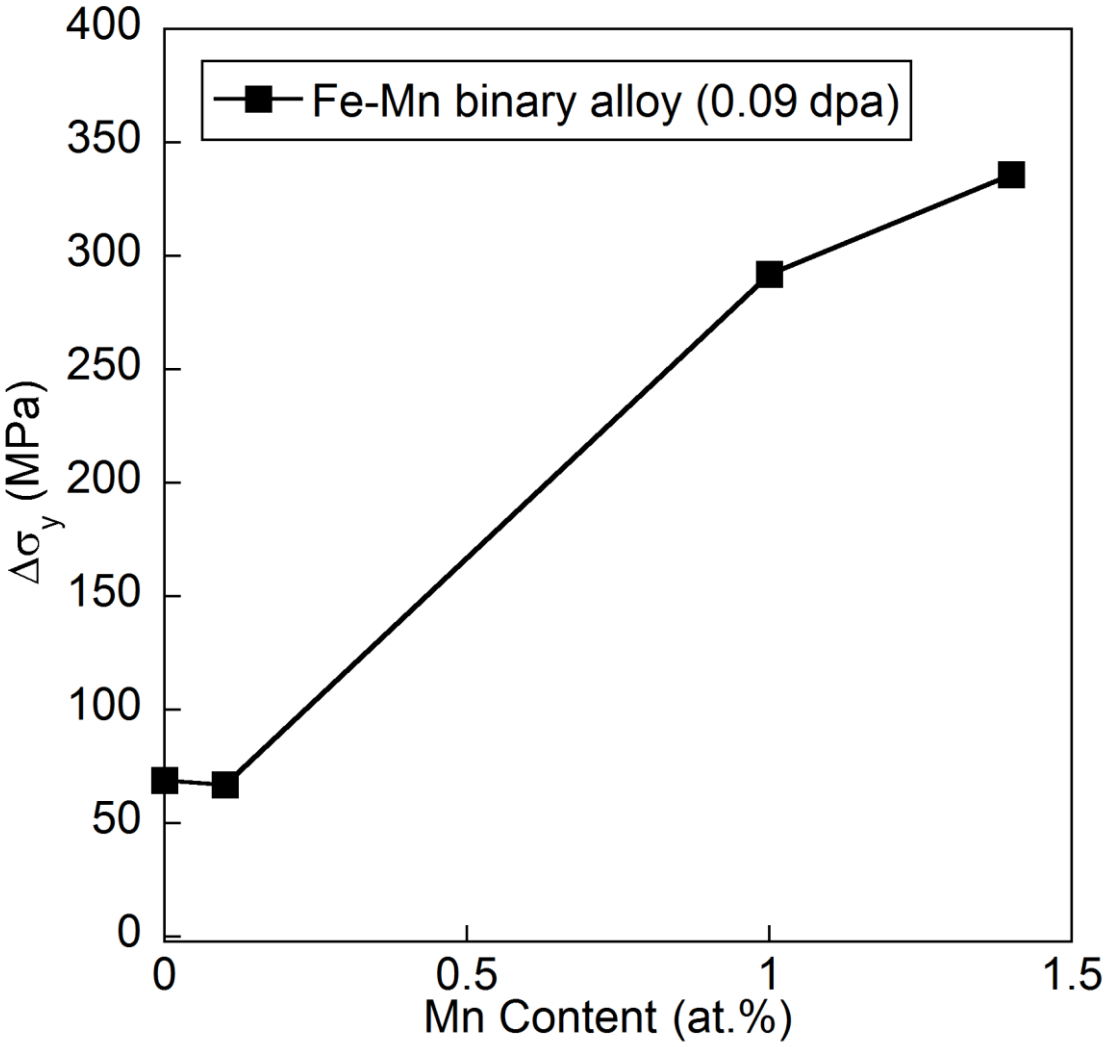
Fe-Mn binary alloy (0.09 dpa)
$\Delta\sigma_y$ (MPa)
400
350
300
250
200
150
100
50
0
0
0.5
1
1.5
Mn Content (at.%)

Fig. 4

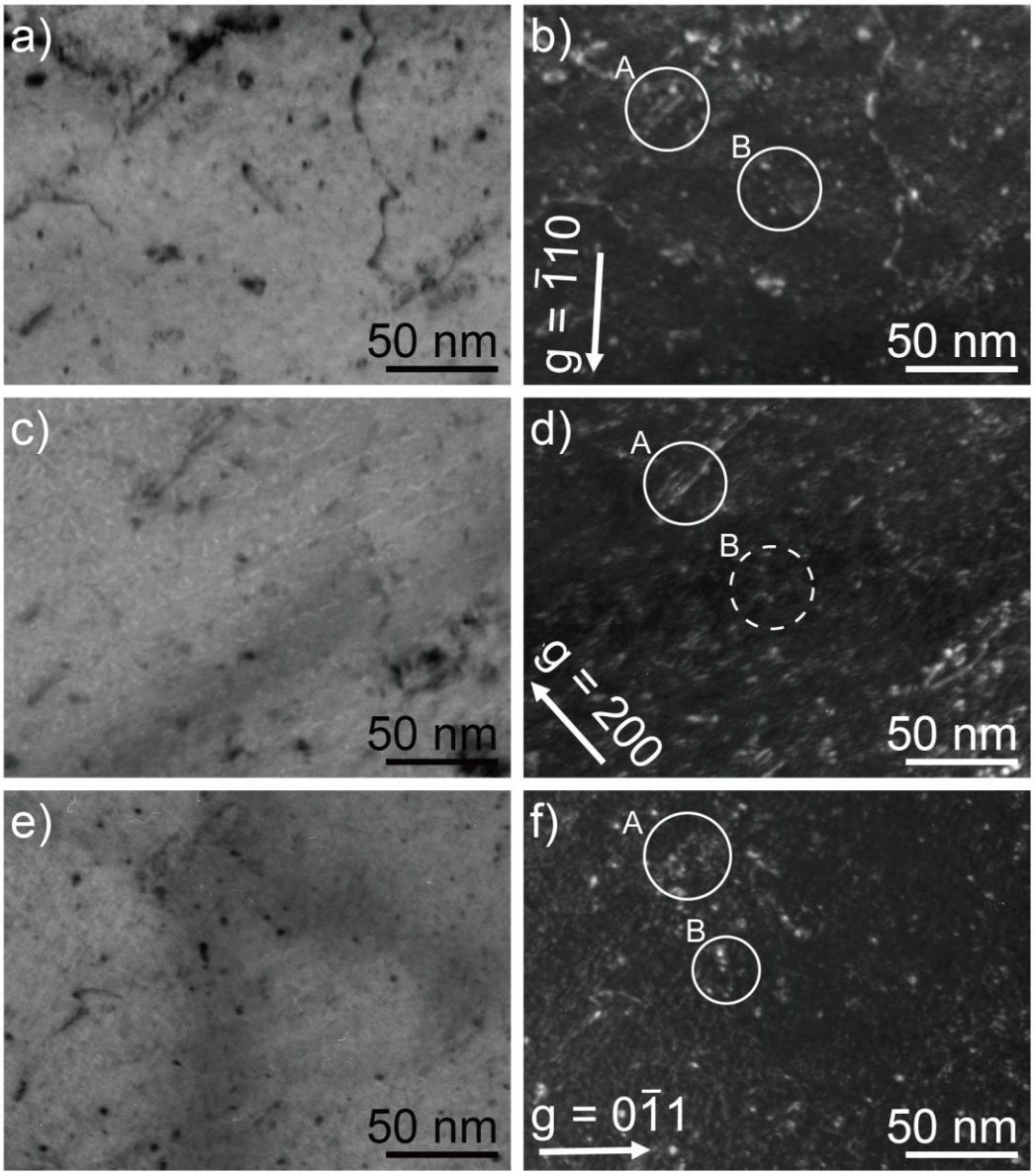

Fig. 5